JOURNAL OF MATERIALS SCIENCE 28 (1993) 2989–2998

Adhesion testing of glass–ceramic thick films on metal substrates

I. A. ASHCROFT*
Department of Physics, Keele University, Staffordshire, UK
B. DERBY
Department of Materials, Oxford University, Parks Road, Oxford, OX1 3PH, UK

The adhesion of thick glass–ceramic films bonded to metal substrates was measured using five different tests: tensile delamination using a bonded stud, scratch testing, an interfacial shear test, indentation and a bend test. All the tests proved to have limitations, and no test gave a fully quantitative measure of adhesion. However, the different tests did rank the samples in the same order of adhesion strength. This indicates that although a fully quantitative method of testing the adhesion of thick films has not yet been developed, many of the published tests can be used to obtain qualitative data.

1. Introduction

When considering the performance and durability of a ceramic-coated component, the adhesion of the coating to the substrate will be an important factor. It is useful, therefore, to be able to measure the strength or fracture toughness of the coating–substrate interface. This measurement is also useful when used in conjunction with microstructural studies of specific interfaces in order to obtain a better understanding of the adhesion mechanisms involved. Although many tests to measure adhesion have been suggested, most are not suitable for the materials being studied and in all cases great care should be taken when interpreting data from these tests in order to distinguish the adhesion element from the contribution of other factors to the result, i.e. to determine exactly what is being measured in the tests.

In the present work five different tests have been used in an attempt to obtain a reliable method of measuring adhesion:

(i) direct pull test,
(ii) scratch test,
(iii) interfacial shear test,
(iv) identation test,
(v) bend test.

In the scratch test and the direct pull test the method is to apply an increasing load or strain to the interface until delamination occurs and to use this load (referred to as the critical load) as a measure of the strength of adhesion of the interface. In the indentation and bend tests a controlled crack is propagated along the interface, and the change in strain energy of the system as the crack advances is used to calculate the fracture toughness of the interface. This is a more fundamental measurement of interfacial adhesion, but care needs to be taken to ensure that the mathematical analysis of the system is an accurate model of what is occurring in the tests. Finally, a test in which the interfacial shear strength is calculated from the maximum crack density achieved in a tensile-loaded sample is assessed.

2. Experimental materials

Thick glass–ceramic films (20–200 μm) were deposited on copper and a copper–Invar–copper (CIC) laminate substrate [1]. Glass–ceramic A was lithium–zinc-silicate based and glass–ceramics B–D were lithium-aluminosilicates with various oxide additions. Deposition of the films was via screen printing and the printed samples underwent a heat treatment to initiate crystallization of the glass–ceramic following wetting of the substrate and densification of the glass.

The fracture toughness of each glass–ceramic was calculated from indentation-induced cracks using the Evans and Charles equation [2]:

$$K_c = 0.0824\, P/c^{3/2} \quad (1)$$

where P is the applied load and c the crack radius. In this investigation indentations were made with a Vickers hardness testing machine. Ten indentations were made on each glass–ceramic with loads of 10–30 kg. Crack lengths were measured with a calibrated optical microscope and verified with a scanning electron microscope and a scanning acoustic microscope.

The average fracture toughness for each glass–ceramic and the experimental variation in the tests are shown in Table 1. It can be seen that the toughness of the glass–ceramics rank in the order A > D > C > B. The experimental variation, however, shows that there is some overlap between the measurements from the different glass–ceramics. It should be pointed out that

*Present address: Department of Materials Science, University of Technology, Sydney, P.O. Box 123, Broadway, NSW 2007, Australia.

0022–2461

TABLE I Fracture toughness of glass–ceramics

Glass–ceramic	Average K_c ($Nm^{-3/2} \times 10^6$)	G_c ($J\,m^{-2}$)
A	2.2 ± 0.2	49
B	1.7 ± 0.3	30
C	1.8 ± 0.3	34
D	2.0 ± 0.4	41

the measurement of fracture toughness from indentation-induced cracks is a complex issue and many models have been proposed. A more complete discussion of the use and limitations of the technique can be found in the literature [1, 3].

3. Adhesion tests

3.1. Direct pull tests

3.1.1. Experimental procedure

In this test an increasing tensile strain is applied to the coating–substrate interface through a glued stud until failure occurs. The failure mode is noted and the adhesion strength is calculated as the critical load divided by the area of coating bonded to the stud.

Discs of glass–ceramic 8 mm in diameter were screen-printed on to metal substrates for testing. The substrates were glued to steel baseplates which were then screwed to the base of the tensometer. An aluminium stud (5 mm diameter) was glued to the top surface of the glass–ceramic coating. All surfaces were etched and/or cleaned in acetone prior to bonding to ensure good adhesion. Testing was carried out at a crosshead speed of $10\,mm\,min^{-1}$. The load was transmitted via a 1 m length of wire cord attached to the load cell and aluminium stud by pinned joints, in an attempt to ensure pure tension and minimize any variation between tests.

3.1.2. Results

Four sets of samples were tested and the results are presented in Table II. In the case of the copper–glass-ceramic A samples, interfacial failure only occurred in two of the nine samples tested. In these cases a heavy oxide layer (Cu_2O) was noted on the copper surface and failure was 100% at the copper–oxide interface. The other samples failed by adhesive failure at the stud or coating surface. The results show that when a heavy oxide was not present the copper–A interface was capable of withstanding tensile stresses in excess of 78 MPa. In the case of the CIC–glass-ceramic D samples it can be seen that of the nine samples tested, seven failed partially at the coating–substrate interface and two failed entirely through the adhesive, thus giving only a lower limit to the interfacial strength. In all cases where coating–substrate failure was observed, mixed failure modes occurred. A schematic representation of a mixed failure mode is shown in Fig. 1. The areas of interfacial failure appeared in discrete spots of variable size from which the crack path deviated upward and outward through the glass–ceramic coating to the free surface, after which failure continued at the coating–adhesive or stud–adhesive interface. The highest value noted for a non-interfacial failure was 57 MPa and interfacial failure occurred in the 35–57 MPa range. Samples 7 and 10 similarly showed mixed failure modes, with some samples exhibiting partial failure at the glass-ceramic–metal interface and in addition some failure within the glass–ceramic itself was noted. The CIC–B interface failed in the 45–80 MPa range, whereas the CIC–C interface showed interfacial failure from 41 to 78 MPa. In both B and C some samples withstood greater stresses before failing in the adhesive or at one of the interfaces with the adhesive.

3.2. Scratch tests

The scratch test is normally used to measure the adhesion of thin films rather than the thick films presently under investigation [4, 5]. However, preliminary trials with a scratch indenter indicated the test was capable of delaminating thick films and therefore may be useful as a means of measuring adhesion. Although various models have been developed to analyse the results from the scratch test [6, 7], none are widely accepted as yet and applicability is even less likely in the case of thick films. The method was used therefore as a means of ranking the adhesion of samples with similar properties rather than as a method of producing a quantitative measure of adhesion strength.

3.2.1. Experimental procedure

Scratch tests were carried out using equipment made at Oxford University. The indenter used was a conical diamond indenter with a tip radius of 0.2 mm and a cone angle of 120°. The sample was held on a double-axis table, which was driven in the scratch direction by a 6 V d.c. servo-motor. A scratch speed of $30\,mm\,min^{-1}$ was used with an average scratch length of 10 mm. The indenter was loaded in the range 0.1–5 kg. After each scratch the table was moved perpendicular to the scratch direction and the applied load increased until failure was noted. Failure was observed during testing by means of an optical microscope. Following testing, a scanning electron microscope (SEM) fitted with an energy-dispersive X-ray spectrometer (EDX) was used to study the surface of selected scratched samples and sections, though some scratch tracks were polished to 1 μm for optical and scanning electron microscopy of the fracture paths in the coatings. These tests validated the optical microscopy observations of the scratches.

3.2.2. Results

The results from the scratch tests are presented in Table III. It can be seen from the table that a number of different failure modes were observed. In all cases the first sign of failure was cohesive flaking at the edges of the scratch channel, as shown in Fig. 2a. This was often accompanied by cracking in the coating. It can be seen from Table III that although the load at which cohesive flaking first occurs varies with

TABLE II Adhesion strengths of glass–ceramic to metal joints by the direct-pull test

Sample No.	Substrate	Glass–ceramic	Failure strength (MPa)	Failure mode (approx. fractions)[a]
6	Copper	A	32	1.0 I ($Cu–Cu_2O$)
			57	0.9 AS, 0.1 AG
			38	0.8 AS, 0.2 AG
			55	1.0 AS
			77	Cord failure
			31	1.0 AS
			78	Cord failure
			50	1.0 AS
			43	1.0 I ($Cu–Cu_2O$)
10	CIC	B	45	0.5 G/I, 0.45 AG, 0.05 AS
			47	0.6 G/I, 0.4 AG
			28	0.5 AS, 0.35 AG, 0.15 G
			80	0.75 AG, 0.15 AS, 0.1 G/I
			60	0.85 AS, 0.1 AG, 0.05 G
7	CIC	C	78	0.45 AS, 0.45 AG, 0.1 G/I
			41	0.9 AS, 0.05 AG, 0.05 G/I
			80	Cord failure
			77	0.8 AS, 0.2 AG
			49	0.1 AS
4	CIC	D	61	0.5 AG, 0.45 AS, 0.05 I
			57	1.0 AS
			77	0.5 AS, 0.5 I, 0.1 AG
			35	0.5 AG, 0.45 AS, 0.05 I
			69	0.4 AS, 0.3 AG, 0.25 I, 0.05 G
			51	0.4 I, 0.3 AS, 0.25 AG, 0.05 A
			35	0.4 I, 0.3 AS, 0.25 AG, 0.05 G
			57	0.8 AS, 0.1 I, 0.05 AG, 0.05 G
			44	0.9 AS, 0.1 AG

[a] AS = adhesive–stud interface,
AG = adhesive–glass-ceramic interface,
I = metal–glass-ceramic interface,
G = within glass–ceramic,
A = within adhesive.

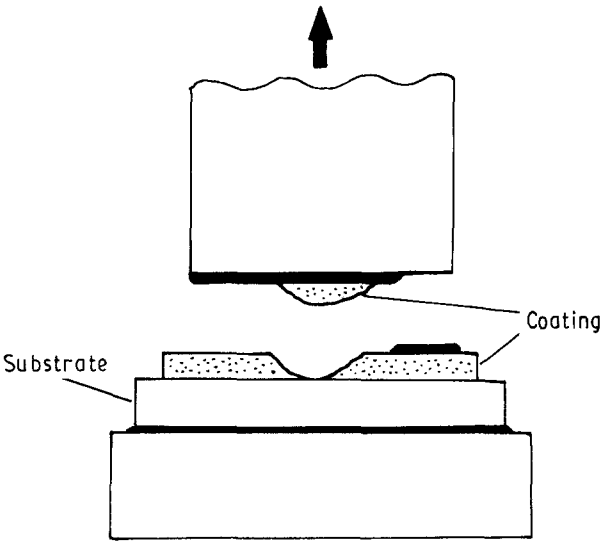

Figure 1 Schematic example of mixed-mode failure in the pull test.

glass–ceramic composition, there is no consistent coating thickness effect. This would imply that the cohesive failure measures a property of the coating to withstand deformation around the indenter which is independent of interfacial adhesion. Once failure has been initiated, the extent of failure will be a function of the fracture toughness of the glass–ceramic and the residual stress field. In the previous section the fracture toughnesses of the glass–ceramics were ranked in the order A > D > C > B, and it can be seen that the same order can be applied to the resistance of the glass–ceramics to cohesive flaking, thus indicating that the load at which cohesive flaking occurs is dependent on the fracture toughness of the glass–ceramic. However, as with the fracture toughness results, there is a degree of overlap in cohesive failure measurements between different glass–ceramics which makes it difficult to pursue this trend with any certainty. The first sign of interfacial failure was either by the appearance of mixed adhesive–cohesive flaking (MACF) at the edges of the scratch channel or by localized areas of coating removal (LCR) within the scratch channel itself. The former failure mode can be seen in Fig. 2b. The failure mode shows no obvious correlation with either coating thickness or glass–ceramic composition. Glass–ceramics A and D failed entirely by MACF, whilst glass–ceramic B failed by LCR with the thinner coatings and MACF with thicker coatings. In the case of glass–ceramic C, the coatings deposited on preoxidized CIC (samples 3 and 18) failed by MACF whereas those on CIC which was heat-treated only (samples 7 and 13) failed by LCR. It was noted that samples from the same firing batch

TABLE III Failure loads of glass–ceramic to metal bonds using the scratch test

Sample No.	Substrate	Glass–ceramic	Coating thickness (μm)	Load (kg)	Failure mode[a]
20	CIC	A	122	0.5	CF
				3.5	MACF
16	Copper	A	50	1.0	CF
				2.0	MACF
				3.0	D
5	Copper	A	125	1.5	CF
				4.0	MACF
				5.0	D
24	Copper	A	155	1.5[b]	CF
10	CIC	B	37	0.5	CF
				1.5	L
				2.0	S
9	CIC	B	40	0.5	CF
				1.0	L
				2.0	S
2	CIC	B	147	0.3	CF
				0.4	MACF
				0.5	D
7	CIC	C	26	0.2	CF
				0.3	L
				1.0	S
3	CIC (OX)	C	71	0.5	CF
				1.5	MACF
				2.0	D
18	CIC (OX)	C	96	0.5	CF
				1.0	MACF
				1.5	L
13	CIC	C	99	1.0	CF
				3.0	L
15	CIC	D	52	1.5	CF
				2.0	MACF + L
4	CIC	D	125	0.5	CF
				2.0	MACF
				5.0	D
20	CIC	D	126	1.0	CF
				3.0	MACF
27	CIC	D	200	1.0[b]	CF

[a] CF = cohesive flaking at sides of scratch channel,
MACF = mixed adhesive–cohesive flaking,
D = coating delaminated at sides of scratch channel,
L = localized coating removal in scratch channel,
S = total coating removal in scratch channel.
[b] No interfacial failure at 5 kg.

tended to fail in the same manner. The load at which either MACF or LCR first occurs will be called the critical load, P_c. When the applied load was increased beyond this point, extensive delamination across the sample or complete removal of the coating in the scratch channel was observed following MACF or LCR, respectively. The former can be seen in Fig. 2c. It can also be seen from Table III that the scratch test was unable to initiate interfacial failure in the case of very thick (> 150 μm), well-adhered coatings at the loads tested. With these samples the coating was observed to be flaking under the scratch stylus and then pushed into the substrate.

In Table III it can be seen that copper–glass-ceramic A samples showed P_c increasing with coating thickness from 2 to > 6 kg. The CIC–A sample exhibited MACF at 3.5 kg, which gives it a similar P_c to that expected from a copper–A sample of similar coating thickness. In the case of glass–ceramic B, P_c appears to decrease as coating thickness increases. This may be misleading, however, as samples 9 and 10 can be viewed as having practically the same coating thickness and scratch behaviour, and sample 2 appears to exhibit anomalously low interfacial adhesion. The CIC–C results should be viewed in terms of the fact that the substrates of samples 3 and 18 were pre-oxidized before coating to develop a continuous oxide interfacial layer, whereas samples 7 and 13 were not. Comparing samples 18 and 13, it appears that better adhesion is attained when the oxide layer is not

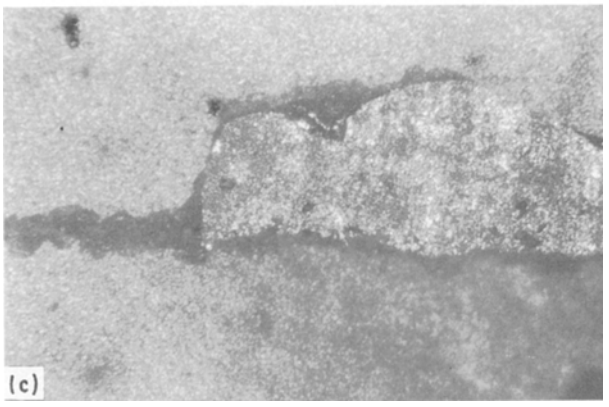

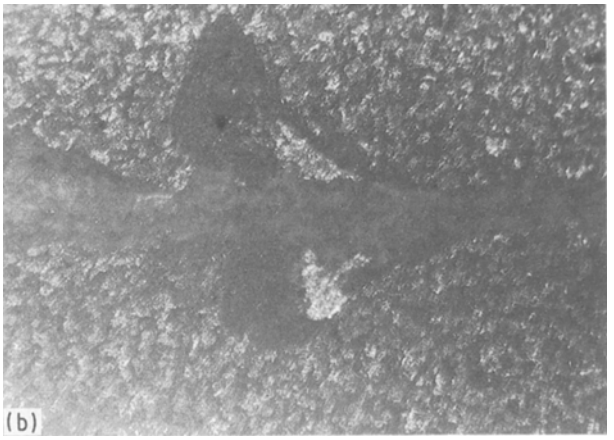

Figure 2 Plan view of scratch tracks: (a) cohesive flaking in sample 3, (b) mixed adhesive–cohesive flaking (MACF) in sample 15, (c) delamination in sample 3. All at 120x.

present. In electron microscopy studies of the samples [1] differences in the development of the interfacial oxide layer in samples 3 and 18 were seen, which may explain why the thinner coating has a larger P_c. CIC–D samples show P_c increasing with coating thickness from 2 kg to > 6 kg.

From the results described above we would rank Cu–A and CIC–A as the systems exhibiting greatest adhesion and CIC–B as the weakest. The picture is more confused in the middle of the ranking order, particularly with the additional complication of the effect of interfacial oxidation layers in the case of glass–ceramic C. On the evidence to date we would put CIC–C and CIC–D on an equal footing except when a continuous oxide layer is present, in which case the adhesion is reduced.

Although the Benjamin and Weaver model [6] was not considered to be directly applicable to the present system, due to the assumption of pure plastic deformation of the substrate and neglect of coating effects, calculations using their model (Equation 2 below) gave interfacial shear strengths of 0.4–1.5 GPa:

$$F = \left(\frac{HW}{\pi[r^2 - (W/\pi H)]}\right)^{1/2} \quad (2)$$

where F is the shearing force per unit area to delaminate the coating given in terms of the substrate hardness H, the critical applied load W and the radius of the stylus point r.

3.3. Interfacial shear strength tests

Agrawal and Raj [8] proposed a method of measuring the shear strength of metal–ceramic interfaces by depositing a ceramic coating on a ductile substrate and pulling the sample in tension. As the sample is pulled cracks, perpendicular to the loading direction appear in the coating. The density of cracks increases with load until a point is reached at which the interface is unable to withstand the degree of deformation required to provoke further cracking. At this point areas of coating between cracks begin to delaminate and spall off the substrate. The maximum crack density in the ceramic coating was shown by Agrawal and Raj to be dependent on the interfacial shear strength, τ, and the following expression was derived using a conventional shear-lag model similar to those used in modelling the subcritical cracking behaviour of fibre-reinforced composites:

$$\tau = \frac{\pi t \sigma}{\lambda} \quad (3)$$

This relates the shear strength to the maximum spacing between cracks, λ (once constant crack density has been reached), the coating thickness, t, and the tensile strength of the film, σ.

3.3.1. Experimental procedure

Two sets of samples were used, copper-coated with glass–ceramic A and CIC-coated with glass–ceramic D. In both cases various thicknesses of coating were tested and in the case of the copper–A system two substrate thicknesses were used. The sample width was 3.2 mm and sample lengths varied from 27 to 33 mm. The samples were tested using an Instron tensile testing machine at a crosshead displacement rate of 0.1 mm min^{-1}. Three samples were tested with each glass–ceramic thickness and at least two of these were strained to such a degree as to attain a constant crack density in the coating. A travelling microscope was stationed at the tensile testing equipment to monitor crack development during testing, and final crack spacing measurements were made on a calibrated optical microscope. Examples of the cracks can be seen in Fig. 3.

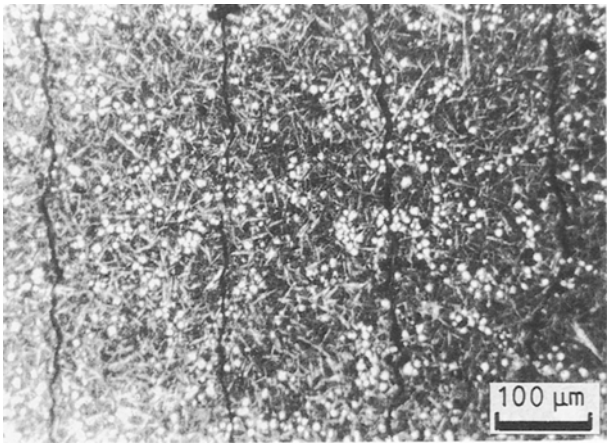

Figure 3 Cracks in glass–ceramic A coating after tensile straining for the shear strength test.

In the thicker films the onset of cracking was easily observable by travelling microscope and stress relief in the load–extension trace. This allowed the failure strain (ε_f) to be measured. The elastic modulus (E) of the glass–ceramic films were measured by acoustic microscope and nanoindenter techniques [9]. The tensile strength of the films were then calculated from E and ε_f.

3.3.2. Results

The interfacial shear strengths of copper–A and CIC–D samples of various coating thicknesses are shown in Table IV. The copper–A interface appears to exhibit the greater shear strength, and there is a general trend of decreasing shear strength with increasing coating thickness, although this is by no means proportional or consistent. This could also be interpreted as decreasing film strength with increasing thickness, which would be expected from the behaviour of brittle materials. The results showed experimental variations of 5–20% in the two or three samples tested, the greatest variation being in the thinner coatings which exhibited the greatest crack density. Without further tests it is impossible to say whether the variation in shear strength with coating thickness is a true one or a product of experimental variation. If τ and σ were constant for a particular coating–substrate combination then maximum crack spacing should be directly proportional to coating thickness. This relationship is plotted in Fig. 4 and can be seen to be true within the accuracy of the test.

3.4. Indentation tests

The fracture resistance of the copper–glass-ceramic interface was investigated using the indentation test developed by Marshall and Evans [10]. In this test an energy balance approach is used to analyse the fracture at coating–substrate interfaces caused by indentations normal to the coating surface. In their model the section above the crack was treated as a rigidly clamped disc and the crack extension force was equilibrated with changes in the strain energy of the system as the crack extended. The following expression for the fracture toughness of the interface (G_c) was derived in terms of the crack diameter a, the indenter load P, the hardness H, Poisson ratio ν, and modulus E of the coating and the residual stress σ_r:

$$\mathscr{C}^2 = \mathscr{P}^2 \frac{(1 + \nu)/2 - (1 - \alpha)(1 - \mathscr{P}^{-1})}{1 - R} \quad (4)$$

where

$$\mathscr{C} = \frac{a^2}{\gamma}\left(\frac{G_c}{E(1 - \nu)t^5}\right)^{1/2}$$

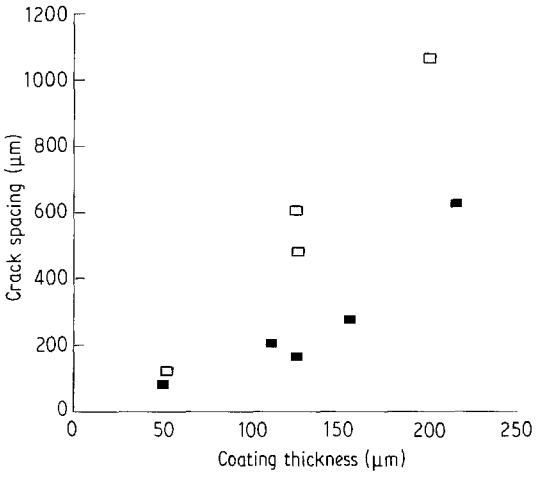

Figure 4 Crack spacing as a function of coating thickness in the shear strength test for two glass–ceramic films: (■) Cu–A, (b) CIC–D.

TABLE IV Ultimate shear strengths of glass–ceramic to metal bond calculated from crack spacings

Sample No.	Substrate	Glass–ceramic	Coating thickness (μm)	Crack spacing (μm)	Shear strength (GPa)
16	Copper	A	50	82	3.6
6			111	204	3.3
5			125	165	4.5
24			155	277	3.3
25			215	628	2.0
15	CIC	D	52	123	2.5
4			125	607	1.2
26			126	483	1.5
27			200	1067	1.1

in which t = coating thickness and

$$\mathscr{P} = \zeta\left(\frac{P}{Ht^2}\right)^{3/2} \qquad \zeta = \frac{\cot\psi}{6\pi 2^{1/2}(1-\nu)\gamma}$$

$$\gamma = k/12(1-\nu^2)$$

where

k = 14.68 and

ψ = 74° for a Vickers indenter;

$$R = \sigma_r^2 \frac{t(1-\alpha)(1-\nu)}{EG_c}$$

where $\alpha = 0.38$ (buckling) or 1 (no buckling). If there are no residual stresses this will reduce to

$$G_c = (2a^4)^{-1} Et^5(\zeta\gamma)^2 (P/Ht^2)^3 (1-\nu^2) \quad (5)$$

3.4.1. Experimental procedure

A Vickers hardness testing machine was used to indent the glass–ceramic coating, with loads of 5–40 kg. The area around the indentation was then examined using optical microscopy. By focusing some distance from the indentation an unfocused disc could be seen around the indentation. This was assumed to be the area of coating buckled upwards due to the presence of the interfacial crack, and the diameter of this disc was taken as a measure of the diameter of the interfacial crack. Sections through indentations were later made and polished to flatness using 1 μm diamond paste for optical microscopy, in order to check this assumption and to characterize crack geometry beneath the indentation. Examples of glass–ceramics B, C, and D bonded to CIC substrates were tested. In the case of copper–glass-ceramic A samples no identation-induced crack could be propagated along the interface.

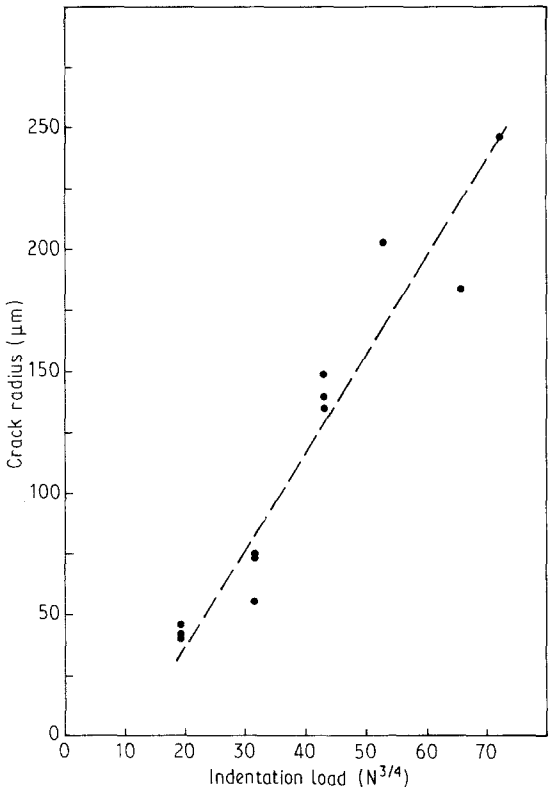

Figure 5 Indentation load to the 3/4 power against crack radius for CIC–glass-ceramic B sample.

3.4.2. Results

A plot of $P^{3/4}$ against a can be seen in Fig. 5 for sample 3. A reasonably straight line can be drawn through these points, affirming the proportionality predicted from Equation 3. Calculations from these results gave fracture energies of 1538, 2624 and 2668 J m^{-2} for glass–ceramics B, C and D, respectively. Fig. 6 shows a section through an indentation in sample 4. It can be seen that in addition to interfacial cracking there is a system of cracks parallel and perpendicular to the interface in the glass–ceramic, which would aid in the release of indenter-induced stresses and account for some of the buckling noted on the surface. In some cases a crack diverted through the glass–ceramic to the free surface was observed. The interfacial cracks seen in cross-sections were approximately the same size as those measured from the surface, though sectioning and polish damage made it difficult to measure crack radii accurately from the cross-sections.

3.5. Bend tests

In this test an interfacial crack is propagated by four-point bend testing a sample as shown in Fig. 7. When the film delaminates there are two components of energy release:

1. The film is on the tensile surface of the beam, experiencing a load P. The strain energy due to this tensile force is given by

$$U_t = \frac{P^2 a}{2E_f bd} \quad (6)$$

where E_f is the Young's modulus of the film.

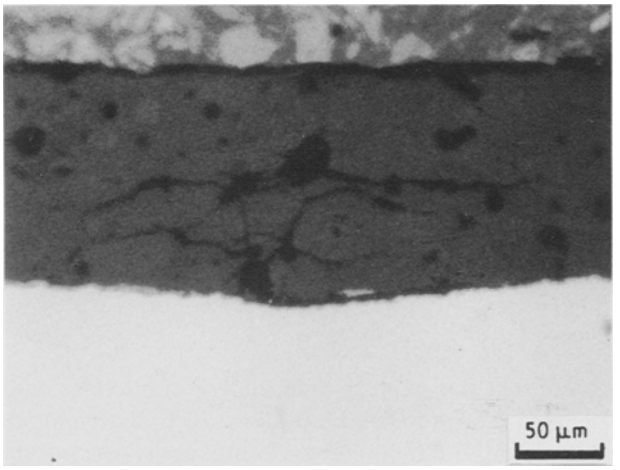

Figure 6 Optical micrographs of cross-sections through 20 kg Vickers indentations in CIC–glass-ceramic D sample.

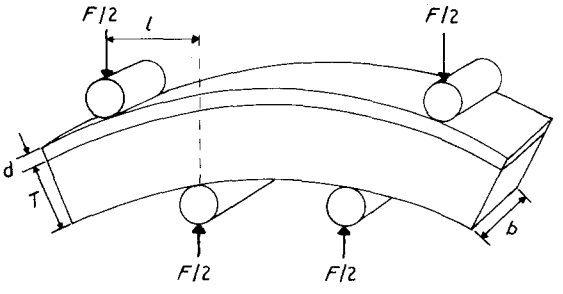

Figure 7 Schematic representation of the bend test.

2. The film is bent by a moment M, such that the strain energy is given by

$$U_m = \frac{1}{2}M\theta = \frac{Ma}{2r} \quad (7)$$

where a = crack length and r = radius of curvature.

To calculate P and M in terms of the applied bending load F, we assume the film is sufficiently thin that it does not affect the rigidity of the beam; then $P \approx \sigma_t bd$, where σ_t is the tensile stress at the top surface of the beam; $\sigma_t = E_f T/2r$ and thus

$$P = E_f Tbd/2r \quad (8)$$

From elementary beam theory

$$M = \frac{I_f E_f}{r} = \frac{E_f bd^3}{12[r + (T/2)]} \quad (9)$$

From Equations 6 and 8

$$U_t = E_f T^2 bda/8r^2 \quad (10)$$

From Equations 7 and 9

$$U_m = E_f bd^3 a/24r^2 \quad (\text{if } r \gg T/2) \quad (11)$$

As the crack extends there is negligible change in total beam deflection. Thus the fixed-grip approximation [11] may be used to calculate the strain energy release rate per unit crack width, G:

$$G = \frac{dU}{da} = \frac{E_f bd}{8r^2}\left(T^2 + \frac{d^2}{3}\right)$$

where

$$r = \frac{I_s E_s}{M_s} = \frac{bT^3 E_s}{12 M_s}$$

so that

$$G = \frac{18 E_f dM_s^2}{bT^6 E_s^2}\left(T^2 + \frac{d^2}{3}\right)$$

$$= \frac{18 E_s dF^2 l^2}{b^2 T^6 E_s^2}\left(T^2 + \frac{d^2}{3}\right)$$

At the critical load F_c we have

$$G_c = \frac{18 E_f dF_c^2 l^2}{b^2 T^6 E_s^2}\left(T^2 + \frac{d^2}{3}\right) \quad (12)$$

Note that this value is independent of interface crack lengths. Thus the bend test allows us to determine the interfacial fracture energy using easily measurable parameters.

3.5.1. Experimental procedure

Prior to four-point bend testing of the sample, it was necessary to establish a crack at the film–substrate interface. This was achieved by indenting the ceramic and then stressing the sample in three-point bending. One side of the sample was polished using 1 μm diamond paste prior to testing and the three-point bend test was carried out under an optical microscope in order to note the point at which an interfacial crack appeared. At this point the test was stopped and the sample was transferred to an Instron tensile testing machine fitted with a four-point bend-test jig. The bending load was increased until a change in the load–extension behaviour of the sample was noted. Optical and scanning acoustic microscopy were then used to determine whether crack propagation had occurred. In addition some samples were tested in four-point loading directly under an optical microscope in order to note crack formation and the strains at which crack propagation occurred. The only samples in which interfacial cracks could be propagated prior to extensive plastic deformation of the substrate were glass–ceramic A films on 2.6 mm thick copper substrates. Samples 25 mm long and 2 mm wide were tested.

3.5.2. Results

The fracture toughness was calculated in the range 3–5 $J\,m^{-2}$. The glass–ceramic coating experiences a tensile stress when the sample is bent (as quantified above) which reaches a maximum value at its surface. This tends to result in the propagation of cracks through the ceramic perpendicular to the film. It can be seen from Fig. 8 that even well-developed interfacial cracks have a tendency to deflect upwards into the coating.

4. Discussion

4.1. Assessment of tests

The pull test was severely limited by the strength of the adhesive used to attach the pin through which the tensile force was applied to the coating. There may be adhesives available which would provide a stronger bond; however, the test is still primarily a comparative one with no quantitative model of interface fracture available.

The scratch test proved to be a promising technique because coating delamination was achieved in most cases, and therefore the test was used to test a wide range of samples. Failure in the scratch test was complex, involving a number of failure mechanisms. The

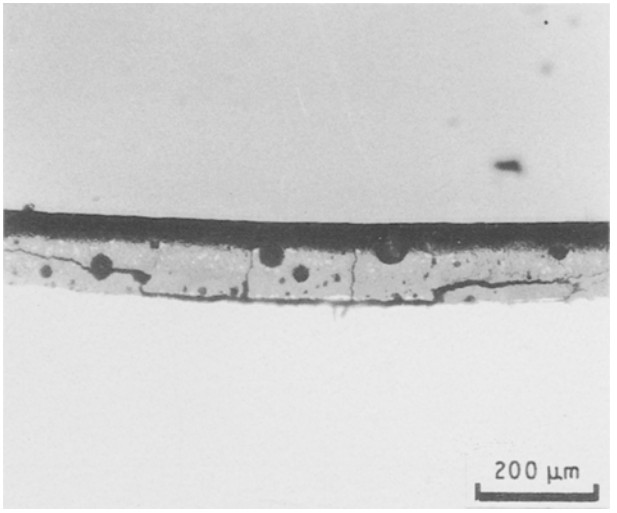

Figure 8 Optical micrograph of a cross-section through a copper–glass-ceramic A bend-test sample.

first sign of coating failure in all cases was cohesive flaking within the coating. This was tentatively linked to the coating's intrinsic bulk fracture toughness, although further work is needed to substantiate this claim. The first sign of interfacial failure was either mixed adhesive–cohesive flaking at the edges of the scratch channel or localized coating delamination in the scratch channel itself. As the load was increased beyond the critical load, either extensive delamination of the coating at the sides of the scratch channel or complete removal of the coating in the scratch channel occurred. No obvious factor determining which failure mechanism occurs in a given system was identified and in some cases both failure modes were observed. Coating thickness appeared to affect the failure load, with a tendency in most cases for the critical failure load to increase with coating thickness. It is obvious that further work characterizing the failure of thick film–substrate systems in the scratch test is needed if a quantitative measure of adhesion is to be developed. The most promising directions for the development of an applicable model of the scratch test are the energy balance and stress component approaches outlined by Burnett and Rickerby [7].

The ultimate shear strength test was promising in that it ranked the samples in the same order as the scratch test. This technique required more material than the other methods used and hence only three tests could be made from each sample. It was difficult, therefore, to measure the range of experimental scatter from so few results; however, the samples that were tested indicated that this could be high, i.e. > 10%. It was also impossible to say whether the observed variations in shear strength with coating thickness were real or merely due to experimental scatter. Only two glass-ceramic–metal systems were investigated with this method, and it would be interesting to further evaluate the technique with relation to other systems.

The indentation test also ranked samples in the same order as the scratch test. Misgivings about the applicability of the theoretical model, however, question the validity of the fracture energies calculated. The main deviations from the model were the extensive cracking in the coating itself and the plastic deformation of the substrate. The problem lies in the strength of the interface in relation to the strength and thickness of the coating. This meant it was impossible to propagate an indentation-induced interfacial crack without deforming the substrate and extensively damaging the coating. This would seem to be an unavoidable problem with the materials studied, and extension of the theory to include these factors would be extremely difficult.

The bend test was only used to test one glass-ceramic–metal system and again, difficulties were experienced in propagating interfacial cracks. However, the results from this test probably give a more realistic estimation of the fracture toughness of the interface. For this reason it is believed that the technique is worthy of further investigation, and further modification of the experimental set-up would probably increase the success of the technique.

4.2. Adhesion strength of glass–ceramic thick films bonded to metal substrates

From the above it can be seen that problems still exist in the measurement of adhesion. It is encouraging that all the tests gave the same order of adhesion to the samples that were tested (Table V). The widest range of samples was measured with the scratch test, which gave the following order for adhesion strength:

$$\text{(Copper, CIC)–A} > \text{CIC–(C, D)} > \text{CIC(ox)–C} > \text{CIC–B}$$

It would appear from this that the composition of glass–ceramic A must result in stronger adhesion than in the lithium aluminosilicate glass–ceramics. The residual stresses in the copper–A system are greater than those in the CIC–B and CIC–C systems, and in the case of the CIC–A samples it was predicted from thermal expansion data that the residual stresses in the coating would be tensile in nature, which would be expected to reduce performance in the scratch test [1]. It is also interesting to note that when etching the glass-ceramic–metal cross-sections the interface etched preferentially in some cases [1]. This could have been due to the existence of residual stresses at the interface, in which case the fact that the CIC–glass-ceramic B interface was most severely etched may be significant as this system proved to have the poorest adhesion. Also the copper–A interface, which had the strongest adhesion, showed least preferential etching at the interface. It can only be concluded from this that the average residual stresses in the coating may be a poor indicator of adhesion strength, and it may be advisable to try and determine residual stresses directly adjacent to the interface.

Measurements of fracture toughness of bulk glass–ceramics gave the same ranking order to the

TABLE V Ranking orders of glass–ceramic to metal bonds from the range of adhesion tests

Adhesion test	Ranking order	Range of results
Pull test	Copper–A > CIC–(B, C, D) > Copper(ox)–A	σ = 32–80 MPa
Scratch test	(Copper, CIC)–A > CIC–(C, D) > CIC(ox)–C > CIC–B	L_c = 0.4–5 kg
Shear strength test	Copper–A > CIC–D	τ = 1.1–3.8 GPa
Indentation test	Copper–A > CIC–D > CIC(ox)–C > CIC–B	G_c = 1.5–2.7 kJ m^{-2}
Bend test	Only CIC–A tested	G_c = 3–5 J m^{-2}

glass–ceramics as adhesion strength, and indeed it can be seen how the failure modes in the scratch test which originate from cracks in the coating would be sensitive to the fracture toughness of the coating. However, as the differences in the fracture toughness of the glass–ceramics were small in comparison with the scatter of the results it is unlikely that this is the controlling factor in adhesion measurements.

Both pull and scratch tests showed that a continuous oxide layer at the interface results in poorer adhesion strength than when discrete oxide precipitates developed. Failure in the former case occurred between the copper and the copper oxide. This indicated that bonding between the copper and the oxide was not as strong as that between the glass–ceramic and the copper oxide or between the copper and the glass–ceramic. Another factor that may contribute to the poor adhesion of the continuous oxide layer to the copper are the residual stresses arising from differential thermal expansion between the copper and the copper oxide. These stresses would increase as the coating thickness increased. The precipitation of copper oxide near the interface indicates high copper concentrations in these regions. This would aid adhesion between the copper and the glass–ceramic via bonding between the copper in the substrate and the coating. In addition a glassy phase was observed between the copper oxide precipitates and the copper [1] which may also aid bond formation and help to relieve interfacial stresses by viscous flow.

References

1. I. A. ASHCROFT, "Characterisation of Glass-Ceramic to Metal Bonds", DPhil thesis, University of Oxford (1991).
2. A. G. EVANS and C. A. CHARLES, *J. Amer. Ceram. Soc.* **59** (1976) 371.
3. C. B. PONTON and R. D. RAWLINGS, *Mater. Sci. Technol.* **5** (1989) 865.
4. A. J. PERRY, *Surf. Eng.* **2** (1986) 183.
5. J. VALLI, *J. Vac. Sci. Tech.* **A4** (1986) 3007.
6. P. BENJAMIN and C. WEAVER, *Proc. Roy. Soc.* **A254** (1960) 163.
7. P. J. BURNETT and D. S. RICKERBY, *Thin Solid Films* **157** (1988) 233.
8. D. C. AGRAWAL and R. RAJ, *Acta Metall.* **37** (1989) 1265.
9. I. A. ASHCROFT, C. W. LAWRENCE, T. P. WEIHS and B. DERBY, *J. Amer. Ceram. Soc. Comm.* **75** (1992) C1284.
10. D. B. MARSHALL and A. G. EVANS, *J. Appl. Phys.* **56** (1984) 2632.
11. B. R. LAWN and R. WILSHAW, in "Fracture of Brittle Solids" (Cambridge University Press, 1975) p. 49.

Received 10 April
and accepted 17 November 1992